To: Students Registered in 720 D30 and 750-D41

From: Z. P. Bažant and J. Planas
"Fracture Mechanics of Concrete"
(in preparation)

6.1 Size Effect in Equivalent Elastic Crack Approximations

6.1.1 Size Effect in the Large Size Range

We have seen in the preceding chapter that at peak load, all the equivalent crack models satisfy (5.3.6). Moreover, for large specimen sizes, the critical equivalent crack extension tends to a limiting constant value c_f: $\Delta a_{ec} \to c_f$ for $D \to \infty$; see (5.3.4).

To find the size effect implied by (5.3.6) in the large size range, we first set in it $\alpha_{ec} = \alpha_0 + c_f/D$ and we solve for σ_{Nu} as

$$\sigma_{Nu} = \frac{K_{Ic}}{\sqrt{D\, k^2(\alpha_0 + c_f/D)}} \tag{6.1.1}$$

We next approximate $k^2(\alpha_0 + c_f/D)$ by its two term Taylor series expansion at α_0:

$$k^2(\alpha_0 + c_f/D) \approx k_0^2 + 2k_0 k_0' \frac{c_f}{D} \tag{6.1.2}$$

where $k_0 = k(\alpha_0)$ and $k_0' = k'(\alpha_0)$ stand for the values of $k(\alpha)$ and its first derivative for the initial crack length. Inserting this approximation into (6.1.1), we get

$$\sigma_{Nu} = \frac{K_{Ic}}{\sqrt{k_0^2 D + 2k_0 k_0' c_f}} = \frac{K_{Ic}}{\sqrt{2k_0 k_0' c_f}\,\sqrt{1 + D/(2k_0' c_f/k_0)}} \tag{6.1.3}$$

so that if we set:

$$B f_t' = \frac{K_{Ic}}{\sqrt{2k_0 k_0' c_f}}, \quad \text{and} \quad D_0 = \frac{2k_0'}{k_0} c_f \tag{6.1.4}$$

we obviously get the classical form (1.4.10) of Bažant's size effect law:

$$\sigma_{Nu} = \frac{B f_t'}{\sqrt{1 + D/D_0}} \tag{6.1.5}$$

With the foregoing derivation we have achieved another independent justification for Bažant's size effect law, and have shown that all the equivalent crack models asymptotically converge to it for large sizes. At the same time we obtained an interpretation of its constants $B f_t'$ and D_0, in terms of the more fundamental fracture parameters K_{Ic} and c_f. The relations (6.1.4) are at the base of the experimental determination of the fracture properties of concrete based on size effect, the main topic in the next sections. Here we use them to explore the structure of the size effect parameters D_0 and B.

The second expression in (6.1.4) reveals the basic characteristics of the transitional size D_0. First, it is proportional to the effective length of the fracture process zone c_f, which in turn is approximately proportional to the inhomogeneity size of the material (dictated by microstructural features), and also to the characteristic size $\ell_{ch} = K_{Ic}^2/f_t'^2$, as discussed in §5.3.1. Second, it is proportional to the ratio $2k'(\alpha_0)/k(\alpha_0)$, which is independent of material properties and introduces the effect of structure geometry (shape). It is interesting to note that this ratio is the same appearing in the definition of the intrinsic size $\overline{D}$ previously introduced in §5.3.3 for the fracture process zone of concrete, and appears in some other works dealing with nonlinear fracture models, particularly those of Horii and Planas and Elices (Horii 1989; Horii, Hasegawa and Nishino 1989; Horii, Shi, and Gong 1989; Planas and Elices 1989, 1990, 1991, 1992; Llorca, Elices and Planas 1989; Elices and Planas 1991, 1992). Though certainly not an exact characterization of structure geometry, this ratio apparently captures its main effect on fracture.

The first of (6.1.4), in turn, reveals the basic structure of B: it can be rewritten in terms of ℓ_{ch} as

$$B = \frac{1}{\sqrt{2k_0 k_0'}} \sqrt{\frac{\ell_{ch}}{c_f}} \tag{6.1.6}$$

which shows that B also consists of a product of a geometrical function times a material parameter. This material parameter was called $\beta = c_f/\ell_{ch}$ in §5.3.1— Eqs. (5.3.3) and (5.3.5)— and is related to the softening behavior of the material; for concrete its value can be estimated in the range 2–5.

6.1.2 Size Effect in the Jenq-Shah Model

To analyze the size effect delivered by the Jenq-Shah model (Bažant199??—discussion of Tang *et al.* 1992)[1] we consider geometrically similar structures (with similar notches) and rewrite the governing equations (5.5.1) and (5.5.10) in parametric form. To simplify the expressions, we drop the subscript from $\Delta\alpha_{ec}$ and write $\alpha_{ec} = \alpha_0 + \Delta\alpha$; then we solve for σ_{Nu} from (5.5.1):

$$\sigma_{Nu} = \frac{K_{Ic}}{\sqrt{D k^2(\alpha_0 + \Delta\alpha)}}, \tag{6.1.7}$$

which, we remark, is identical to (6.1.1), except that $\Delta\alpha$ is not given, but must be obtained from (5.5.10), which we leave as it was (except for the subscript):

$$\Delta\alpha\, L^2(\Delta\alpha, \alpha_0) = \frac{c_f}{D} \tag{6.1.8}$$

[1] Zdenek: please complete this reference.

where c_f is given in terms of the material properties E', K_{Ic} and w_{Tc} by (5.5.11). The two foregoing equations are the parametric equations of the size effect curve for the Jenq-Shah model. Elimination of the parameter $\Delta\alpha$ delivers the size effect curve σ_{Nu}–D.

This elimination is not feasible analytically in general. However, the solution for relatively large sizes can be found by expanding the equations in series of powers of $\Delta\alpha$ and c_f/D. To do so, we remark that $L(c_f/D, \alpha_0)$ is regular in c_f/D and accepts a power series expansion; therefore, so does $L^2(c_f/D, \alpha_0)$ and one can write, recalling that $L(0, \alpha_0) = 1$:

$$L^2(\Delta\alpha, \alpha_0) = 1 + \sum_{n=1}^{\infty} a_n (\Delta\alpha)^n \tag{6.1.9}$$

where for brevity we do not make explicit that the coefficients a_n depend on α_0.

Now, one may seek a power expansion solution of (6.1.8) by writing

$$\Delta\alpha = \frac{c_f}{D} + \sum_{n=1}^{\infty} b_n \left(\frac{c_f}{D}\right)^{n+1} \tag{6.1.10}$$

where the b_n's are determined substituting (6.1.9) and (6.1.10) into (6.1.8) and identifying the coefficients of c_f/D on both sides of the equal sign. One easily finds the first few terms of the expansion: $b_1 = -2a_1$, $b_2 = 2a_1^2 - 3a_2, \ldots$.

Now we go back to (6.1.7) and expand $k^2(\alpha)$ in Taylor series at $\alpha = \alpha_0$

$$k^2(\alpha_0 + \Delta\alpha) = k_0^2 \left[1 + c_1\Delta\alpha + c_2(\Delta\alpha)^2 + \ldots\right] \quad , \text{ where } \quad c_n = \frac{1}{k_0^2 n!} \frac{d^n k^2(\alpha)}{d\alpha}\bigg|_{\alpha=\alpha_0} \tag{6.1.11}$$

Finally, we substitute this and $\Delta\alpha$ given by (6.1.10) into (6.1.7), and obtain the following expression for the size effect corresponding to the Jenq-Shah model:

$$\sigma_{Nu} = B f_t' \left[1 + \frac{D}{D_0} + d_1 \frac{c_f}{D} + d_2 \left(\frac{c_f}{D}\right)^2 + \ldots\right]^{-1/2} \tag{6.1.12}$$

where B and D_0 are the same as defined in (6.1.4), and d_n are coefficients that may be obtained in terms of the coefficients b_n and c_n. The first two coefficients are, for example: $d_1 = (c_1 b_1 + c_2)/c_1$, and $d_2 = (c_1 b_3 + 2c_2 b_1 + c_3)/c_1$.

Equation (6.1.12) represents a general asymptotic description of the size effect of the Jenq-Shah model. This infinite asymptotic series is similar to that derived in Bažant (1986) by another argument (see Chapter 10). For not too small size D, the terms with c_f/D, $(c_f/D)^2$, etc. are negligible compared to 1. Dropping them, we see that (6.1.12) reduces to the size effect law in (6.1.5).

So we may conclude that the equivalent LEFM model based on the critical crack-tip opening displacement, including Jenq and Shah's two-parameter model for concrete, gives a size effect that is asymptotically equivalent to the size effect law, Eq. (1.4.10) or (6.1.5). This conclusion implies that Jenq and Shah's model must give overall similar results as the R–curve model base on the size effect law. Furthermore, it follows that the material parameters of Jenq and Shah's model can be determined from size effect measurements.

6.2 Size Effect Law in Relation to Fracture Characteristics

6.2.1 Defining Objective Fracture Properties

Experience shows that different experimental techniques or different analysis (i.e. using different models for the interpretation of the tests results) may lead to different values of nominally identical fracture parameters: fracture toughness, fracture energy, size of the fracture process zone, etc. There is, however, a way to uniquely define such parameters: Use the values of the parameters corresponding to the extrapolation of specimen size to infinity. The reason: As discussed in the preceding chapter, in an infinitely

large specimen, the fracture process zone occupies an infinitely small fraction of the specimen volume. Therefore, in the limit, all of the specimen volume is in an elastic state; and since from linear elastic fracture mechanics it is known that the near–tip asymptotic field of displacements and stresses is the same regardless of the shape and size of the specimen or structure, it turns out that the fracture process zone in an infinitely large specimen is exposed along its boundary to the same stress or displacement field, regardless of the specimen shape, and so it must behave in the same manner. In particular, it must have (statistically) the same distribution of strains and microcracks, the same length and width, and the same energy dissipation. Consequently, an unambiguous definition (proposed by Bažant1987a) is as follows:

The fracture energy G_f and the effective fracture process zone length c_f are, respectively, the energy release rate required for crack growth and the distance from the notch tip to the tip of the equivalent LEFM crack in an infinitely large specimen of any shape (provided it has positive geometry).

Without the foregoing asymptotic definition, the problem of defining and determining the material fracture characteristics becomes ambiguous and more difficult. The fracture process zone length and width depends on the specimen shape because it is influenced by the proximity of the specimen boundary. It appears impossible to eliminate from measurements these parasitic influences with high accuracy without making an extrapolation to infinite size.

Because the failure of specimen (peak load) is dictated by the material characteristics, it must be possible to determine these characteristics from size effect measurements. In fact, by virtue of the foregoing asymptotic definition, the determination of fracture characteristics is reduced to the calibration of the size effect law. If we knew this law exactly, we would get exact results. But the exact size effect law, applicable up to arbitrarily large sizes, is not known. Therefore, the size effect method, like others, yields in practice only approximate results. Nevertheless, the validity of Bažant's size effect law (6.1.5) is rather broad, covering a size range of up to about 1:20, which suffices for most practical purposes. We shall see in the next chapter that other extrapolations lead to different values for parameters named identically; however, if the values are used consistently (i.e., within the modles on which their obtention is based), then similar predictions are obtained for typical aspects of the structural response (peak load, load–displacement curves or the like). We next determine the relation of the parameters in Bažant's size effect law with the more fundamental fracture parameters.

6.2.2 Determination of Fracture Parameters from Size Effect

In the previous section we showed that the size effect dictated by effective crack models converge to Bažant's size effect law for infinite size, and we determined the relation of the size effect parameters D_0 and Bf'_t with the asymptotic fracture parameters, Eqs. (6.1.4).

Thus, if we assume that D_0 and Bf'_t are known from experiment (see the next section for the detailed experimental procedures), we can solve for K_{Ic} and c_f from (6.1.4) and get

$$K_{Ic} = Bf'_t\sqrt{D_0}k_0 \tag{6.2.1}$$

$$c_f = \frac{k_0}{2k'_0}D_0 \tag{6.2.2}$$

For infinite size, LEFM must hold, and according to Irwin's relationship, $G_f = K_{Ic}^2/E'$, so from (6.2.1) we get

$$G_f = \frac{(Bf'_t)^2 D_0 k_0^2}{E'} \tag{6.2.3}$$

6.2.3 Intrinsic Representation of the Size Effect Law

In the foregoing, the size of the specimen, D, is just a 'user-selected' (i.e. arbitrary) linear dimension. It turns out, then, that different users can obtain different size effect parameters. Thus, these parameters are not intrinsic and cannot be directly compared if different D are used or, more important, different geometries are involved.

The concept of intrinsic size introduced in §5.3.3, allows rewriting Bažant's size effect law (6.1.5) in

an intrinsic form in which the geometrical and material properties are decoupled (Bažant and Kazemi 1990a). Setting in (6.1.3) that $D/(2k_0'/k_0) = \overline{D}$ —in accordance with the definition (5.3.11) of the intrinsic size $\overline{D}$— we get

$$\sigma_{Nu} = \frac{K_{Ic}}{\sqrt{2k_0k_0'(c_f + \overline{D})}} \tag{6.2.4}$$

so that if we introduce the intrinsic nominal strength $\overline{\sigma}_{Nu}$ defined as

$$\overline{\sigma}_{Nu} = \sigma_{Nu}\sqrt{2k_0k_0'} \tag{6.2.5}$$

we get a modified size effect law in which the parameters depend only on material properties:

$$\overline{\sigma}_{Nu} = \frac{\overline{B}f_t'}{\sqrt{1 + \overline{D}/\overline{D}_0}} \tag{6.2.6}$$

and

$$\overline{B}f_t' = \frac{K_{Ic}}{\sqrt{c_f}}, \qquad \overline{D}_0 = c_f \tag{6.2.7}$$

Thus, if the size effect is expressed in terms of the intrinsic strength $\overline{\sigma}_{Nu}$ and of the intrinsic size $\overline{D}$, the structure of the equation is retained, but the dependence on the geometry (shape) of the specimen is eliminated. This allows using data from different specimens shapes and sizes in a single plot, a fact that can be useful to compare apparently dissimilar results.

Exercises

6.1 Determine K_{Ic}, G_f and c_f for test series B1 and C1 in Section 1.5. Sort the materials by (1) strength and (2) toughness. Note: Estimate the Young modulus from ACI formula $E = 4735\sqrt{f_c'}$. Take $k_0 = 0.687$ and $k_0' = 2.10$ (the method to obtain them will be explained in §6.3.4).

6.2 According to (6.2.6), for a given intrinsic size $\overline{D}$, the behavior is fully brittle (i.e., LEFM applies exactly) when $c_f = 0$, and the behavior is fully ductile when $c_f \to \infty$. We may define a material brittleness γ as the inverse of c_f: $\gamma = 1/c_f$ (with unit m^{-1} or mm^{-1}). Compute the material brittleness for series B1 and C1.

6.3 Size Effect Method: Detailed Experimental Procedures

6.3.1 Outline of the Method

In the size effect method, a number of geometrically similar notched specimens of various sizes are tested for peak load. The nominal strength is then computed and plotted versus the size, and the values of the parameters Bf_t' and D_0 are obtained by best fitting of the size effect law to the experimental results. Finally, K_{Ic}, G_f and c_f are obtained from Eqs. (6.2.1)–(6.2.3).

It should be noted that the size effect method is applicable only for specimens of positive geometry, i.e., those for which $k'(\alpha_0)$ is positive. When $k'(\alpha_0)$ is approximately zero or negative, the method is inapplicable. This happens, for example, during the initial crack growth in a center–cracked specimen loaded on the crack. One reason for the failure of the size effect method is that in such specimens the crack length at maximum load can be much longer than the notch, due to stable crack growth, and thus the crack lengths at maximum loads of specimens of different sizes are not similar. Another reason is that Eq. (6.2.2) gives in this case either infinite or negative c_f which is impossible.

Eqs. (6.2.1)–(6.2.3) are used for regressions based on the size effect law in its ordinary form (6.1.5). One can, however, also use the size effect law in the intrinsic form (6.2.6), which directly involves material parameters G_f and c_f. In that case, these parameters can be obtained directly by optimal fitting of Eq. (6.2.6) to the measured values of $\overline{\sigma}_{Nu}$ for various values of $\overline{D}$. When such a method is used, the

specimen shapes do not necessarily have to be geometrically similar, and test results for different specimen geometries can be mixed in one and the same regression. However, the parameter that takes into account the specimen shape, namely the ratio $k'(\alpha_0)/k(\alpha_0)$, is only approximately known and thus it introduces an additional error. To avoid this error, it is preferable to use specimens that are geometrically similar.

In either case, the fitting can be accomplished easily by nonlinear regression using some nonlinear optimization subroutine such as Levenberg–Marquardt algorithm. One advantage of this procedure is that this subroutine also gives the coefficients of variation of G_f and c_f. However, other simpler methods involving linear regression can be used too. In the next section we examine the simplest regression procedures.

6.3.2 Regression Relations

In a latter section, we shall justify that the best approach to identifying D_0 and Bf_t' from experiments is nonlinear optimization, provided that a computer subroutine such as Levenberg-Marquardt algorithm is available. From measurements one gets a series of nominal strength values σ_{Nu_k} corresponding to sizes $D_k (k = 1, 2, \ldots)$ and values of D_0 and Bf_t' are sought such that the quadratic deviations in a log–log plot are minimum (Fig. 6.3.1a). This is equivalent to a fit in classical coordinates (x, y) in which the curve to fit is written as

$$y = \ln \frac{M}{\sqrt{N + \exp(x)}} \tag{6.3.1}$$

where

$$x = \ln D, \; y = \ln \sigma_{Nu}, \;\; Bf_t' \sqrt{D_0} = M, \;\; D_0 = N \tag{6.3.2}$$

One readily gets K_{Ic}, G_f and c_f in terms of the best fit parameters M and N from Eqs. (6.2.1)–(6.2.3):

$$K_{Ic} = k_0 M \,, \quad G_f = \frac{k_0^2}{E'} M^2 \,, \quad c_f = \frac{k_0}{2k_0'} N \tag{6.3.3}$$

Note that M and N have been chosen so that G_f depends on M only and c_f only on N. In this way, the errors for the fit parameters, computed automatically by the optimization routine, can be directly used to estimate the errors for G_f and c_f. If other parameters are used, their correlation coefficient must be also calculated, which is not a standard feature in many commercial optimization routines.

If a nonlinear optimization program is unavailable, one can exploit the fact that the size effect in Eq. (1.4.10) can be algebraically rearranged to a linear regression plot (Bažant 1984; Fig. 6.3.1b):

$$Y = AX + C \qquad \text{Linear Regression I} \tag{6.3.4}$$

for which

$$X = D, \; Y = \left(\frac{1}{\sigma_{Nu}^2} \right), \;\; Bf_t' = \frac{1}{\sqrt{C}}, \;\; D_0 = \frac{C}{A} \tag{6.3.5}$$

As before, K_{Ic}, G_f and c_f follow from Eqs. (6.2.1)–(6.2.3):

$$K_{Ic} = k_0 \frac{1}{\sqrt{A}} \,, \quad G_f = \frac{k_0^2}{E'} \frac{1}{A} \,, \quad c_f = \frac{k_0}{2k_0'} \frac{C}{A} \tag{6.3.6}$$

Another algebraic rearrangement of Eq. (1.4.10) yields an alternative linear regression plot (Planas and Elices 1989; Fig. 6.3.1c):

$$Y' = A'X' + C' \qquad \text{Linear Regression II} \tag{6.3.7}$$

in which

$$X' = \frac{1}{D}, \; Y' = \frac{1}{\sigma_{Nu}^2 D}, \;\; Bf_t' = \frac{1}{\sqrt{A'}}, \;\; D_0 = \frac{A'}{C'} \tag{6.3.8}$$

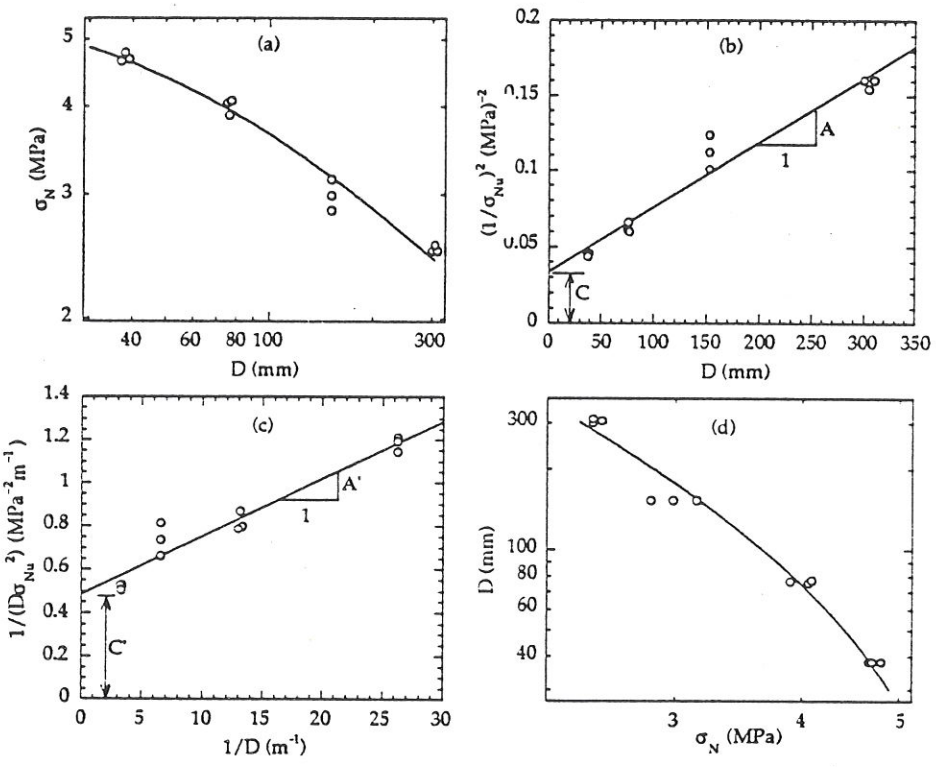

FIGURE 6.3.1
Regression plots: (a) bilogarithmic; (b) linear regression I; (c) linear regression II; (d) Inverse bilogarithmic plot. Experimental data correspond to tests by Bažant and Pfeiffer (1987) reported as Series B1 in Chapter 1 (see tables 1.1 and 1.2).

Now the expressions for K_{Ic}, G_f and c_f are:

$$K_{Ic} = k_0 \frac{1}{\sqrt{C'}}, \qquad G_f = \frac{k_0^2}{E'} \frac{1}{C'}, \qquad c_f = \frac{k_0}{2k_0'} \frac{A'}{C'} \tag{6.3.9}$$

Note that in the first type of linear regression, the fracture energy is inversely proportional to the regression slope, and in the second type of regression, it is inversely proportional to the intercept. The linear regression plot of type I gives a better visual display of the test data for smaller specimen sizes while the regression plot of the type II gives a better display of the extrapolation to infinite size. LEFM corresponds to $c_f \to 0$, that is to $C = 0$ in the first type of regression (line through the origin), and to $A' = 0$ in the second type of regression (a horizontal line). The strength theory corresponds to $D_0 \to \infty$, that is to $A/C = 0$ in the first type of regression (a regression line with a negligible slope), and to $C'/A' = 0$ in the second type of regression (a regression line through the origin).

The regressions in Eqs. (6.3.1), (6.3.4) and (6.3.7) are not completely equivalent and do not yield exactly the same results. The reason is that these regressions imply different weighing of the data points. An improved regression method taking weights into account will be introduced in §6.3.6. Before we examine the RILEM recommendation —which uses the linear regression of type I with equal weights—, we apply the foregoing regressions to an example.

Example 6.3.1 The following table summarizes the results of the tests on notched three-point bend concrete beams by Bažant and Pfeiffer (1987); they correspond to Series B1 in Tables 1.1 and 1.2. From the raw data in the first two rows, the coordinates (x, y), (X, Y) and (X', Y') have been computed according, respectively, to Eqs. (6.3.2), (6.3.5) and (6.3.8) and are included in the following rows of the table.

		specimen No.											
Var.	Units	#1	#2	#3	#4	#5	#6	#7	#8	#9	#10	#11	#12
D	mm	38	38	38	76	76	76	152	152	152	305	305	305
σ_{Nu}	MPa	4.65	4.69	4.79	3.89	4.06	4.08	2.84	2.99	3.15	2.50	2.50	2.55
x	ln(mm)	3.64	3.64	3.64	4.33	4.33	4.33	5.03	5.03	5.03	5.72	5.72	5.72
y	ln(MPa)	1.54	1.55	1.57	1.36	1.40	1.41	1.05	1.09	1.15	.915	.915	.935
$10^3 X$	m	38	38	38	76	76	76	152	152	152	305	305	305
$10^3 Y$	MPa^{-2}	46.2	45.5	43.6	66.1	60.8	59.9	124	112	101	160	160	154
X'	m^{-1}	26.2	26.2	26.2	13.1	13.3	13.0	6.56	6.56	6.56	3.33	3.23	3.28
Y'	$(\text{MPa}\sqrt{\text{m}})^{-2}$	1.21	1.19	1.14	.867	.798	.786	.811	.735	.662	.526	.526	.506

The foregoing values were fed to a commercial data analysis program, which drew the graphics in Fig. 6.3.1 and computed the best fit values for (M, N), (A, C) and (A', C') according, respectively, to the nonlinear regression (6.3.1), the linear regression I (6.3.4) and the linear regression II (6.3.7). With units MPa and m, the results were: $M = 1.46, N = 0.0596, A = 0.427, C = 0.0334, A' = 0.0267, C' = 0.486$. From these, values proportional to K_{Ic}, G_f and c_f were computed from (6.3.3), (6.3.6) and (6.3.9); the following table summarizes the results; the values in parentheses are the coefficient of variation in percent, as delivered by the program.

		Regression		
Parameter	Units	Nonlinear	Linear I	Linear II
$(1/k_0)\, K_{Ic}$	$\text{MPa m}^{1/2}$	1.46 (± 3.4%)	1.53 (± 3.4%)	1.43 (± 3.4%)
$(E'/k_0^2)\, G_f$	$(\text{MPa})^2$ m	2.13(± 6.8%)	2.34(± 6.8%)	2.06 (± 6.8%)
$(2k_0'/k_0)\, c_f$	mm	60 (± 16%)	78 (± 22%)	55 (± 14%)

We see that the values for K_{Ic} have little statistical error (less than 4%), but the values delivered by the three methods differ slightly, the maximum difference relative to the nonlinear fit being about 5%. This difference is twice as large for G_f (because of the squaring) and becomes as large as 30% for c_f. Note, however, that the statistical error is also very large for c_f and that the relative difference between any two results is always lower than twice the coefficient of variation. □

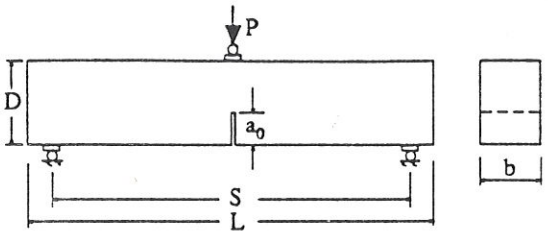

FIGURE 6.3.2
Suggested specimen geometry of the RILEM draft recommendation.

6.3.3 RILEM Recommendation Using the Size Effect Method: Experimental Procedure

One of the RILEM Recommendations on concrete fracture recommends determining the material fracture characteristics from the size effect law (RILEM 1990). The idea of this method, proposed by Bažant (1989) and Bažant and Pfeiffer (1987), is that one first determines the parameters of the size effect law the linear regression I and then the material fracture parameters ensue from Eqs. (6.3.6).

The method works equally well for a number of geometries (provided they are positive geometries), but three-point-bend beams are recommended for the purpose of standardization (Fig. 6.3.2). The loads and reactions are applied through one hinge and two rollers with a minimum possible rolling friction, and through stiff bearing plates (of such a thickness that they could be considered as rigid). The bearing plates are either glued with epoxy or are set in wet cement. The distance from the end of the beam to the end support must be sufficient to prevent spalling and cracking at beam ends. The span–to–depth ratio of the specimen, S/D, should be at least 2.5 (this has been set only for the purpose of standardization; the theory does not prevent smaller values). The ratio of the notch depth to the beam depth, a_0/D, should be between 0.15 and 0.5. The notch width at the tip should be as small as possible and must not exceed 0.5 d_a where d_a = maximum aggregate size. The width b of the beam and the depth d should not be less than $3d_a$.

An important point is the choice of specimen sizes $D_k (i = 1, 2, \ldots n)$ for which the tests should be carried out. If only two sizes were used, the regression line could be passed through the average of the σ_{Nu}-values for each size exactly, and thus one would have no idea how well the observed dependence on D agrees with the size effect law. Therefore, at least three different sizes must be used.

To decide how to choose the specimen sizes D_k optimally, it is helpful to consider inverting the coordinates (Fig. 6.3.1d). One may regard σ_{Nu_k} as the given coordinates, and the corresponding D_k as the size values for which each σ_{Nu_k} would be obtained[2]. These D_k values will in general differ from the D–value corresponding to the size effect law. Therefore, $\Delta D_k = D_k - D$ are the errors (Fig. 6.3.1d). Now, for the same reasons as before, it seems reasonable to consider that the inverse of the size effect law has roughly constant relative errors $\Delta D_k/D_k$ rather than constant absolute, errors ΔD_k. Consequently, since $\Delta D_k/D_k = \Delta(\ln D_k)$, a logarithmic size scale should be used. This means that the sizes D_k of the specimens to be tested should be chosen uniformly spaced in the logarithmic scale. In other words, D_k should form a geometric progression, i.e. $D_1/D_2 = D_2/D_3 = \cdots$. Note that if, on the other hand, the chosen sizes are crowded in one position of the ln D scale, one in fact imposes a bias for that portion of the size range.

In summary, the Recommendation indicates that specimens of at least three different sizes, characterized by beam depths $D = D_1, \ldots D_n$ must be tested. The smallest depth D_1 must not exceed $5d_a$ and the largest depth D_n must not be smaller than $10d_a$. The ratio D_n/D_1 must be at least 4. The ratios of the adjacent sizes, D_{i+1}/D_k, should be approximately constant. Optimally, the size range should be as broad as feasible. Thus, for instance, the choice $D/d_a = 4, 8, 16$ is usually acceptable, but the choices $D/d_a = 3, 6, 12, 24$ or $3, 9, 27$ are preferable.

For statistical reasons, at least three identical specimens should be tested for each specimen size. All the specimens of all the sizes must be cast from the same batch of concrete, and the quality of concrete

[2]**Zdenek:** I still feel uncomfortable with this reasoning. However, I can't find a solid argument either pro or con. I think that stating that geometric progression has been chosen in the recommendation is enough, and this paragraph could be skipped

must be as uniform as possible. The curing procedure and the environments to which the specimens are exposed, including their histories, must be the same for all the specimens. To avoid differences in the hydration heat effects and minimize other types of size effect (see Sec. 1.3), all the specimens should be geometrically similar in two dimensions, that is, the third dimension (thickness b) should be the same for all the specimens.

It is sufficient to use an ordinary uniaxial testing machine without high stiffness. However, closed–loop control and high stiffness of the loading frame lead to more consistent results, and they also permit determining the post–peak response, which is useful for calibration of more sophisticated fracture models. The same machine ought to be used for testing all of the specimens. The specimens should be loaded at constant (or almost constant) displacement rates (this could be the load-point displacement, but better the crack mouth opening displacement). Although the size effect law is applicable over a very broad range of loading rates (its applicability has been demonstrated for tests at which the maximum loads are reached in times ranging from 1 s to 10^6 s; see Chapter 12), for the purpose of standardization it is desirable that the maximum load be reached in about 5 minutes.

Aside from the aforementioned maximum load values $P_1, \dots P_n$ for specimens of sizes $D_1, \dots D_n$, the following data should also be obtained and reported: Young's modulus E_c, standard compression strength f'_c; all the dimensions of the beam and bearing plates; the maximum aggregate size; the ratios (by weight) of water:cement:sand and gravel in the mix; the type of cement, its fineness, and admixtures; the mineralogical type of aggregate; the curing and storing conditions; temperature and relative humidity during the test; and the mean mass density of the concrete.

6.3.4 RILEM Recommendation Using the Size Effect Method: Calculation Procedure

The raw data for the calculations are the specimen dimensions, particularly the beam depths D_k and the measured maximum loads $P^0_{u_k}$ ($k = 1, 2, \dots, n$; n = number of specimens). The first step is to compute σ_{Nu} for all the specimens. For heavy specimens, the own weight of the specimens may have to be taken into account. To this end, the measured maximum loads $P^0_{u_1}, \dots, P^0_{u_n}$ should best be corrected in such a manner that the corrected loads $P_{u_1}, \dots, P_{u_n}$ without own weight would produce the same stress intensity factor according to LEFM. This is approximately equivalent to requiring that the bending moments at the notch section produced by loads $P^0_{u_k}$ plus the own weight be equal to the bending moment due to P_{u_k} alone. For the most usual testing configuration in which the notch is located at the bottom of the beam, if the specimen length L_k is almost the same as the span S_k, and no ancillary equipment (loading plates or rods, e.g.) is resting on the specimen, this is approximately achieved by taking $P_k = P^0_k + (m_k g/2)$ ($i = 1, \dots, n$), in which g is the acceleration of gravity and $m_k g$ = the weights of all the individual specimens. If L_k differs from S_k substantially, then

$$P_{u_k} = P^0_{u_k} + m_k g(2S_k - L_k)/2S_k \tag{6.3.10}$$

From these corrected ultimate loads, the nominal strength of each specimen is computed from the first of (1.4.1). In the original recommendation, $c_N = 1$ is used, and the shape factors for the stress intensity are modified accordingly. Here we use a different value of c_N so that the expressions in chapters 2–5 can be directly used. Specifically, the nominal strength is computed for each specimen as

$$\sigma_{Nu_k} = \frac{3P_{u_k}S_k}{2b_k D_k^2} \qquad k = 1, 2, \dots, n \tag{6.3.11}$$

Finally, one calculates the coordinates of the data points in the linear regression of type I, Eq. (6.3.4) $X_k = D_k$ and $Y_k = (1/\sigma_{Nu_k})^2$ where D_k are the sizes corresponding to P_{u_k}. An example of such correlation is shown in Fig. 6.3.1b.

The slope A and intercept C of the regression line may now be calculated from the well known linear regression equations (e.g. Pugh and Winslow 1966, §11.6; Press et al. 1992, §15.2). For future convenience, we use here a presentation of the equations in a form slightly different from that used in the RILEM (1990) Recommendation. In this presentation it is useful to define the following sums (which are automatically performed by most hand calculators):

$$\Sigma = \sum_{k=1}^{n} 1^k = n\,, \quad \Sigma_x = \sum_{k=1}^{n} X_k\,, \quad \Sigma_y = \sum_{k=1}^{n} Y_k$$
$$\Sigma_{xx} = \sum_{k=1}^{n} (X_k)^2\,, \quad \Sigma_{xy} = \sum_{k=1}^{n} Y_k X_k\,, \quad \Sigma_{yy} = \sum_{k=1}^{n} (Y_k)^2 \tag{6.3.12}$$

Then the regression coefficients A and C are obtained as

$$A = \frac{\Sigma\Sigma_{xy} - \Sigma_x\Sigma_y}{\Delta}, \qquad C = \frac{\Sigma_{xx}\Sigma_y - \Sigma_x\Sigma_{xy}}{\Delta} \tag{6.3.13}$$

where

$$\Delta = \Sigma\Sigma_{xx} - (\Sigma_x)^2 \tag{6.3.14}$$

Note that in the foregoing Y_k are the measured data (not the averages of the data for each size!). It should be checked whether the plot of all the data points is approximately linear (if not, the test procedure was probably jarred by some errors or inadequate control of test conditions).

After computing A and C one calculates the geometrical factors $k_0 = k(\alpha_0)$ and $k_0' = k'(\alpha_0)$ using the shape factor function $k(\alpha)$ given in the recommendation. Three shape functions are given, for span-to-depth ratios $S/D = 2.5$, 4 and 8. Although interpolation is deemed acceptable, the recommendation suggests to stick to these values to avoid introducing additional errors. Today, these expressions can be advantageously replaced by the general formulas of Pastor et al. (1995) given in examples 3.1.1 and 3.1.4 —Eqs. (3.1.1)–(3.1.3) and (3.1.8). We summarize them here for the reader's convenience: The shape factor for a span to depth ratio S/D takes the form

$$k_{S/D}(\alpha) = \sqrt{\alpha}\,\frac{p_{S/D}(\alpha)}{(1+2\alpha)(1-\alpha)^{3/2}}\,, \quad p_{S/D}(\alpha) = p_\infty(\alpha) + \frac{4D}{S}[p_4(\alpha) - p_\infty(\alpha)] \tag{6.3.15}$$

where the polynomials $p_4(\alpha)$ and $p_\infty(\alpha)$ are given by Eqs. (3.1.2) and (3.1.3). With the values of k_0 and k_0' computed from these formulae, the fracture parameters are calculated from (6.3.6). Note that numerical differentiation is the faster method to obtain k_0'; analytic differentiation is feasible, but the resulting formula is too long to be practical.

It is also desirable to calculate statistics of the results. If the standard deviation of the data is not known, an estimate of it is obtained from the quadratic deviation from the straight line, χ^2:

$$\chi^2 = \sum_{k=1}^{n} (Y_k - \hat{Y}_k)^2 = \sum_{k=1}^{n} (Y_k - AX_k - C)^2 = \Sigma_{yy} - A\Sigma_{xy} - C\Sigma_y \tag{6.3.16}$$

Then, the coefficients of variation of A and C —ω_A and ω_C— and the relative width of the scatter band m are determined as

$$\omega_A^2 = \frac{1}{A^2}\,\frac{\chi^2\Sigma}{(n-2)\Delta}\,, \quad \omega_C^2 = \frac{1}{C^2}\,\frac{\chi^2\Sigma_{xx}}{(n-2)\Delta}\,, \quad m^2 = \frac{(n-1)\chi^2\Sigma(\Sigma_x)^2}{(n-2)\Delta(\Sigma_y)^2} \tag{6.3.17}$$

According to the recommendation, the value of ω_A should not exceed about 10% and the values of ω_C and m about 20%. These conditions prevent situations in which the size range is insufficient compared with the scatter of test results. Such a situation is illustrated in Fig. 6.3.3a in which a unique slope can still be obtained but is highly uncertain. Fig. 6.3.3b illustrates the case where large scatter of test results necessitates the use of a very broad size range, while Fig. 6.3.3c illustrates the case where a small scatter of test results permits the use of a narrow size range. Obviously, the necessary breadth of the size range can be reduced by carefully controlled testing which yields low scatter.

From the coefficients of variation of the parameters of the regression line, the coefficients of variation of the fracture parameters can be estimated. The basic equation for the spread of errors is that, if $\zeta = f(\xi_j)$ is a function of N *uncorrelated* random variables ξ_j, $(j = 1, 2, \cdots, N)$, then the coefficient of variation

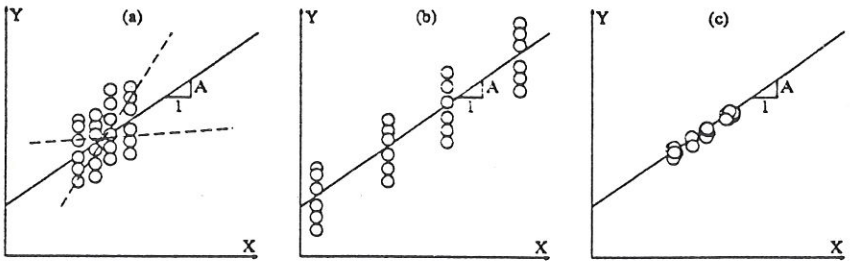

FIGURE 6.3.3
Unacceptable (a) and acceptable (b–c) scatter of the results (adapted from Bažant and Pfeiffer 1987)

verifies the relation

$$\omega_\zeta^2 = \frac{1}{\zeta^2}\sum_{j=1}^{N}\left[\frac{\partial f(\xi_i)}{\partial \xi_j}\right]^2 \xi_j^2 \omega_{\xi_j}^2 \tag{6.3.18}$$

Thus, for K_{Ic} and G_f which, according to (6.3.6), depend respectively on A, and on A and E (which, can be viewed as uncorrelated because they are obtained in different tests), the coefficients of variation are simply given by

$$\omega_{K_{Ic}} = \frac{1}{2}\omega_A\ , \qquad \omega_G = \sqrt{\omega_A^2 + \omega_E^2} \tag{6.3.19}$$

For c_f things are a little bit more complicated, because C and A are not uncorrelated. It is well known that if we write the regression line in the form $Y = A(X - \bar{X}) + \bar{C}$ where $\bar{X} = \Sigma_x/\Sigma$ is the abscissa of the centroid of the data points, then A and $\bar{C}$ are uncorrelated. Obviously $\bar{C}$ is the Y intercept at the centroid, and it is very easy to show that $\bar{C}$ does indeed coincide with the Y coordinate of the centroid of the data points:

$$\bar{C} = \frac{\Sigma_y}{\Sigma} \tag{6.3.20}$$

Furthermore, the coefficient of variation of $\bar{C}$ is given by

$$\omega_{\bar{C}} = \frac{\chi^2 \Sigma}{(n-2)(\Sigma_y)^2} \tag{6.3.21}$$

Now, since $C = A\bar{X} + \bar{C}$, it turns out that $C/A = \bar{X} + \bar{C}/A$ so that from (6.3.6) and (6.3.18) we get

$$\omega_{c_f}^2 = \frac{1}{(C/A)^2}\left[\left(\frac{\bar{C}}{A}\right)^2 \omega_A^2 + \left(\frac{\bar{C}}{A}\right)^2 \omega_{\bar{C}}^2\right] = \frac{\bar{C}^2}{C^2}(\omega_A^2 + \omega_{\bar{C}}^2) \tag{6.3.22}$$

Example 6.3.2 Consider again Bažant and Pfeiffer's results analyzed in example 6.3.1, and apply to them the foregoing analysis. We first construct the sums in (6.3.12): $\Sigma = 12, \Sigma_x = 1.7145, \Sigma_{xx} = 0.37015, \Sigma_y = 1.1335, \Sigma_{yy} = 0.13099, \Sigma_{xy} = 0.21544$, and then compute $\Delta = 1.5023$ from (6.3.14). Next the values of A and C follow from (6.3.13): $A = 0.427, C = 0.0334$; they coincide, as they should, with the values obtained with the commercial program in example 6.3.1. Now, according to the data in Table 1.1, the span-to-depth ratio was $S/D = 2.5$ for series B1. Thus, from (6.3.15) $p_{2.5}(\alpha) = 1.6p_4(\alpha) - 0.6p_\infty(alpha)$, and using the expressions (3.1.2) and (3.1.3) for p_4 and p_∞ we get

$$p_{2.5}(\alpha) = 1.847 - \alpha[-0.1424 + 0.6960(1-\alpha) - 0.4308(1-\alpha)^2 + 1.221(1-\alpha)^3] \tag{6.3.23}$$

and since the relative notch depth was $\alpha_0 = 1/6$ (see Table 1.1), the value of k_0 is readily obtained from (6.3.15): $k_0 = 0.687$. To obtain k_0' we use the numerical approximation $k_0' \approx [k(1/6+0.005) - k(1/6-$

TABLE 6.1
Best fits of G_f and c_f for the results of Bažant and Pfeiffer (1987).

Series	Material	Specimen[a] type	E^b (MPa)	$k_0{}^c$	K_{Ic} (MPa$\sqrt{\text{m}}$)	G_f (N/m)	ω_A (%)	$\omega_{K_{Ic}}$ (%)
B1	concrete	SEN-TPB	27.7	0.673	1.03	38.4	6.8	3.4
B2	concrete	DEN-EC	29.0	1.30	1.14	44.5	7.0	3.5
B3	concrete	DEN-T	25.5	0.832	0.96	35.9	14.8	7.4
C1	mortar	SEN-TPB	32.9	0.673	0.84	21.4	4.1	2.1
C2	mortar	DEN-EC	32.8	1.30	0.86	22.6	4.9	2.5
C3	mortar	DEN-T	32.4	0.832	0.86	22.9	10.0	5.0

[a]See specimen types in Fig. 1.5.1

[b]Calculated from ACI formula $E = 4735\sqrt{f'_c}$

[c]Calculated by FEM by Bažant and Pfeiffer (1987)

$0.005)]/0.01$ and get $k'_0 = 2.10$. Next, (6.3.6) delivers $K_{Ic} = k_0/\sqrt{A} = 0.687/\sqrt{0.427} = 1.05$ MPam$^{1/2}$, $c_f = (k_0/2/k'_0)C/A = (0.687/2/2.1) \times 0.0334/0.427 = 0.0128$ m, or $c_f = 12.8$ mm. To determine G_f we need E, which was not directly determined in Bažant and Pfeiffer's work. We can approximate E by ACI formula $E = 4734\sqrt{f'_c}$, which, using the value $f'_c = 34.1$ MPa from Table 1.2, delivers $E = 27.6$ GPa, from which $G_f \approx 39.9$ N/m. For the statistics, we first compute χ^2 from the last of (6.3.16), which gives $\chi^2 = 1.060 \times 10^{-3}$; then, from (6.3.17) we get $\omega_A = 6.8\%$, $\omega_C = 15.4\%$ and $m = 14.7\%$, and from (6.3.21) $\omega_{\bar{C}} = 3.2\%$, with $\bar{C} = 0.09446$ from (6.3.21). According to this and Eq. (6.3.19), the coefficient of variation of K_{Ic} is $\omega_{K_{Ic}} = 3.4\%$; finally, from (6.3.22) we get $\omega_{c_f} = 22\%$. The coefficient of variation of G_f is *at least* 6.8%; the coefficient of variation of E cannot be obtained from the original Bažant and Pfeiffer's data, so neither can the coefficient of variation of G_f. □

6.3.5 Performance of the Size Effect Method

The fact that determination of G_f and c_f from size effect tests based on Eqs. (6.2.3) and (6.2.2) yields approximately the same results for specimens of very different geometries has been verified by Bažant and Pfeiffer (1987). In their tests, three-point-bend specimens, double edge-notched tension specimens and eccentric compression specimens of size ratios 1:2:4:8 were tested. The essential information about these tests is given in Chapter 1; they correspond to Series B1–B3 for concrete, and C1–C3 for mortar. The optimal fits of the test results are shown in Fig. 1.5.3. The values of the fracture toughness and fracture energy obtained by the regressions of the test results are given in Table 6.1. The critical effective crack extension was not computed in Bažant and Pfeiffer's original work.

It is remarkable that, despite the very different specimen geometries used, the coefficients of variation of K_{Ic} values obtained for specimens of various geometries were, on average, less than 5% (which is better than the scatter of strength test results). It may also be noted that studies of Karihaloo and Nallathambi (1991??), and Swartz and Refai (1987) further indicated that this method yields systematic results free of size and shape effect, and that it also yields for the fracture energy similar results as Jenq and Shah's two parameter method (see Section 5.5).

Karihaloo and Nallathambi (1991??) listed most of the fracture test results known at that time, in which they compared their method (see §5.4.3) to Bažant's size effect method. For this purpose they converted G_f to K_{Ic} according to the LEFM relationship $K_{Ic} = \sqrt{G_f E}$. For the beam tests they reported, the K_{Ic} values were 0.847—0.892 kNm$^{-3/2}$ for the size effect method and $K_{Ic} \approx 0.867$ kNm$^{-3/2}$ for their method. A similar agreement was found for the data of Bažant and Pfeiffer (1987). The size effect method was used by Brühwiller (1988), Saouma et al. (1989??) and He et al. (1992) to measure the fracture energy of dam concrete.

On the other hand, the fracture energy value obtained by these methods is generally quite different from that obtained from the RILEM work of fracture method (RILEM 1985; Hillerborg 1985); see Chapter 7 for a discussion on the sources of the discrepancy.

6.3.6 Improved Regression Relations

As already pointed out, the regressions in Eqs. (6.3.1), (6.3.4) and (6.3.7) are not completely equivalent and do not yield exactly the same results because these regressions imply different weighting of the data points. If consistent weighting is used, then the difference between the three regressions is only marginal, as we show next.

The basic idea in the following is that in the frame of the maximum likelihood theory, the classical least square fitting in which the function $\chi^2 = \sum_k (Y_k - \hat{Y}_k)^2$ is minimized, assumes that the (standard) errors of the various measurements are identical (Y is the theoretical expression for Y as a function of X and the regression parameters). However, in practice this condition can very well not hold, because, for example, the errors are proportional to the measured quantity (constant coefficient of variation), or different load cells have been used to perform the measurements for different X, or else Y is not the measured value but a nonlinear function of it, etc. In such an event, *weighted* least square fitting must be performed. In such weighted regression, the function to be minimized is

$$\chi^2 = \sum_{k=1}^{n} w_k (Y_k - \hat{Y}_k)^2 \tag{6.3.24}$$

where the weights w_k must be inversely proportional to the square of the error (or variance) of the corresponding measurement:

$$w_k \propto \frac{1}{s_k^2} \approx \frac{1}{\omega_k^2 Y_k^2} \tag{6.3.25}$$

in which s_k is the standard deviation for the kth measurement and ω_k its coefficient of variation (the last expression is only approximate because we use the approximate value Y_k instead of the unknown true value of the variable).

The determination of s_k or ω_k for a particular experimental setup is not a trivial matter, and is very rarely carried out in detail. The most usual assumption is that the directly measured quantity (in our case the nominal strength σ_{Nu}) has a constant relative error, i.e., a constant coefficient of variation $\omega_{\sigma_{Nu}}$. Taking this assumption for granted, the weights for the various regressions become fixed. Indeed, using the formula (6.3.18) for the propagation of errors we get the following relationships for the coefficients of variation of the regression variables $y = \ln \sigma_{Nu}$, $Y = 1/\sigma_{Nu}^2$, and $Y' = 1/(D\sigma_{Nu}^2)$:

$$\omega_y = \frac{\omega_{\sigma_{Nu}}}{y}, \qquad \omega_Y = 2\omega_{\sigma_{Nu}}, \qquad \omega_{Y'} = 2\omega_{\sigma_{Nu}} \tag{6.3.26}$$

Thus, the weights to be used for the various regressions are

$$w_k \propto \frac{y_k^2}{\omega_{\sigma_{Nu}} y_k^2} \propto 1 \quad \text{for logarithmic nonlinear regression} \tag{6.3.27}$$

$$w_k \propto \frac{1}{2\omega_{\sigma_{Nu}} Y_k^2} \propto \frac{1}{Y_k^2} \quad \text{for linear regression I} \tag{6.3.28}$$

$$w_k \propto \frac{1}{2\omega_{\sigma_{Nu}} Y_k'^2} \propto \frac{1}{Y_k'^2} \quad \text{for linear regression II} \tag{6.3.29}$$

The foregoing analysis shows that the equal weight assumption is only valid for the logarithmic nonlinear regression; for the other two regressions, the weights must be inversely proportional to the square of the dependent variable Y or Y'. More generally, it shows how the weights in the three regressions are inter-related, and that given any one set of weights the other two sets are fixed.

For the reasons just explained, it is better to use either a logarithmic nonlinear regression or a weighted linear regression to obtain G_f and c_f by the size effect method. If a linear regression of type I is used then we introduce for these points the weights $w_k = 1/Y_k^2$ $(k = 1, \ldots n)$.

The weighted regression formulas are entirely similar to those for equal weights. The only change is

that the sums Σ, Σ_x, etc., defined in (6.3.12) are now redefined as weighted sums as follows:

$$\Sigma = \sum_{k=1}^{n} w_k \,, \quad \Sigma_x = \sum_{k=1}^{n} w_k X_k \,, \quad \Sigma_y = \sum_{k=1}^{n} w_k Y_k$$
$$\Sigma_{xx} = \sum_{k=1}^{n} w_k (X_k)^2 \,, \quad \Sigma_{xy} = \sum_{k=1}^{n} w_k Y_k X_k \,, \quad \Sigma_{yy} = \sum_{k=1}^{n} w_k (Y_k)^2 \tag{6.3.30}$$

This is the only modification: the expressions for Δ, A, C, $\bar{C}$, χ^2 and the coefficients of variation are identical to the formulas in §6.3.4, except that the Σ's appearing in those formulas are now given in (6.3.30).

Example 6.3.3 Consider again Bažant and Pfeiffer's results analyzed in example 6.3.1, and apply to them the weighted linear regression I. We first construct the sums in (6.3.30): $\Sigma = 2620.5$, $\Sigma_x = 189.25$, $\Sigma_{xx} = 23.448$, $\Sigma_y = 160.75$, $\Sigma_{yy} = 12$, $\Sigma_{xy} = 16.097$, and then compute $\Delta = 25630$ from (6.3.14). Next the values of A and C follow from (6.3.13): $A = 0.459$, $C = 0.0282$; they are sensibly different from the values obtained with the equal-weight regression in examples 6.3.1 and 6.3.2. Now, using the values for k_0 and k_0' found in example 6.3.2 we get $K_{Ic} = k_0/\sqrt{A} = 0.687/\sqrt{0.459} = 1.01$ MPam$^{1/2}$, $c_f = (k_0/2/k_0')C/A = (0.687/2/2.1) \times 0.0282/0.459 = 0.01005$ m, or $c_f = 10.0$ mm. Using for E the ACI estimate $E = 27.6$ GPa, computed in example 6.3.2, we get $G_f = K_{Ic}^2/E \approx 37.3$ N/m. For the statistics, we first compute χ^2 from the last of (6.3.16), which gives $\chi^2 = 7.9857 \times 10^{-2}$; then, from (6.3.17) we get $\omega_A = 6.2\%$ and $\omega_C = 9.6\%$, and from (6.3.21) $\omega_{\bar{C}} = 2.8\%$, with $\bar{C} = 0.061343$ from (6.3.21). According to this and Eq. (6.3.19), the coefficient of variation of K_{Ic} is $\omega_{K_{Ic}} = 3.1\%$; finally, from (6.3.22) we get $\omega_{c_f} = 14.9\%$.

Note how the coefficients of variation have decreased with respect to the equal-weight solution: this is because the weighted regression minimizes the relative deviations from the theoretical curve rather than the absolute deviations. □

Example 6.3.4 It is instructive to compare the solutions for the various regressions applicable to Bažant and Pfeiffer series B1. Without detailing the computations (which follow the steps illustrated in the preceding examples), the results for K_{Ic} and c_f and their coefficients of variation are included in the following table:

	Regression				
Parameter	Nonlinear	Linear I	Linear II	Weighted I	Weighted II
K_{Ic} (MPa m$^{1/2}$)	1.00	1.05	0.98	1.01	1.01
c_f (mm)	9.8	12.8	9.00	10.0	10.0
ωK_{Ic} (%)	3.4	3.4	3.4	3.1	3.1
ω_{c_f} (%)	16	22	14	15	15

We see that the two weighted linear regressions and the nonlinear regression deliver nearly the same values and coefficients of variation. Indeed, it is easy to prove that the two weighted linear regressions are in fact identical, with $C' = A$ and $A' = C$. The proof is left as an exercise. □

Exercises

6.3 Compute k_0 and k_0' for the test series run on SEN-TPB specimens of those included in Section 1.5. Use the size effect parameters shown in Table 1.2 to deduce the fracture properties K_{Ic}, G_f and c_f for the various materials. Sort the materials in increasing order of (a) strength, (b) toughness, (c) brittleness.

6.4 The experimental results of Bažant, Gettu and Kazemi for the limestone specimens described in Section 1.5 were as shown in the following table:

		specimen No.											
Var.	Units	#1	#2	#3	#4	#5	#6	#7	#8	#9	#10	#11	#12
D	mm	13	13	13	25	25	25	51	51	51	102	102	102
P_u	N	82	85	78	134	140	140	238	243	243	418	405	394

(a) Determine Bf_t' and D_0 from the linear regression I. (b) Same for weighted regression I. (c) Same for weighted regression II. (d) Compare with the results of the nonlinear logarithmic regression shown in Table 1.2. (e) Calculate K_{Ic}, G_f and c_f.

6.5 Prove that the weighted versions of the linear regressions I and II are identical, with $C' = A$ and $A' = C$. (Hint: write the weighted sum of squares to be minimized for regressions I and II; then set the variables of the second in terms of the variables of the first.)

6.6 Consider the nonlinear logarithmic regression written as $y = -\frac{1}{2}\ln[A\exp(x) + C]$ with $y = \ln\sigma_{Nu}$ and $x = \ln D$. Show that this approaches the weighted linear regression I (or II) if $Y_k - AX_k - C \ll Y_k$. (Hint: write the weighted sum of squares to be minimized for the nonlinear regression; then set the variable (y, x) in terms of (Y, X) and write that $\ln(1+\epsilon) \approx \epsilon$ for $\epsilon \ll 1$.)

6.4 R-Curve Determination Based on Size Effect

As discussed in the previous chapter, the R–curves, which serve as a basis of the equivalent linear elastic fracture analysis, can be determined in various ways which give similar results but are not completely equivalent (§5.6.5). The most recent method is the determination from the size effect data on the maximum loads of geometrically similar specimens of different sizes.

The advantage of the size effect method is that, by definition, the R–curve obtained is size independent, yet it seems to have a very broad applicability, and to be particularly good for prediction of the maximum loads because it is determined on the basis of the maximum loads. All R–curves strongly depend on the structural geometry, although the same R–curve can be used as an approximation for different but very close geometries.

There is a more profound advantage of the size effect method. If the R–curves are determined from data on the load deflection or other similar curves, such data are very sensitive to specimen geometry and size, thus, there is no way to go from one geometry to another except by repeating measurements. The size effect law, on the other hand, has not only, by definition, size-independent parameters, but has also the same shape for very different geometries. This fact has been extensively proven by experiments as well as numerical calculations (within the size range of 1:20, which suffices for most practical purposes). Thus, using the size effect law, one can get at least the shapes of the R–curves for all geometries, in fact without any further testing. Only those parameters of the size effect law which are translated into the parameters of the R–curve need to be calibrated for different geometries. Let us now get the equations for the R–curve from the size effect curve.

6.4.1 Determination of R–curve from Size Effect

Consider that the maximum load P_u has been measured for a set of geometrically similar specimens of different size D. For each size, and each effective crack length a, the energy release ratio at peak load $\mathcal{G}_u$ can be calculated from Irwin's relationship K_I^2/E' as

$$\mathcal{G}_u(a) = \frac{1}{E'}\sigma_{Nu}^2 D k^2(\alpha) \tag{6.4.1}$$

where $\alpha = a/D$ and $k(\alpha)$ is the shape factor for K_I, same for all sizes D. On each curve $\mathcal{G}_u(a)$, there is normally one and only one point that represents the failure point (critical state). At that point, the $\mathcal{G}(a)$ curve must be tangent to the R–curve (see §5.6.3). Consequently, the R–curve must be the envelope of the family of all the fracture equilibrium curves $\mathcal{G}(a)$ for different sizes, as shown in Fig. 6.4.1 (see example in the following for details).

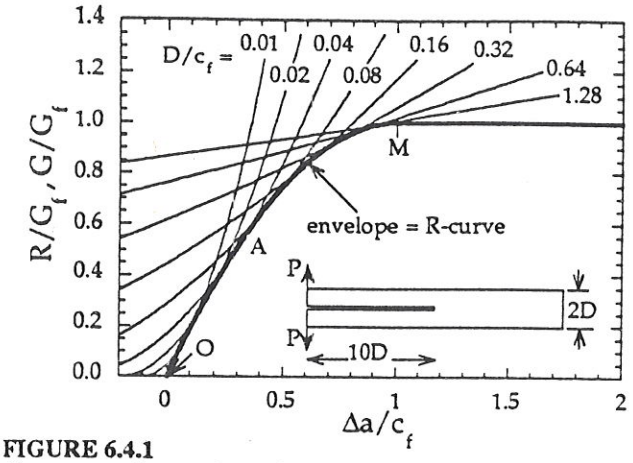

FIGURE 6.4.1
***R*–curve as the envelope of the energy release ratio curves at peak for various sizes.**

To describe the envelope mathematically, let us assume that the size effect law is known. This means that the ultimate nominal stress σ_{Nu} is a known function of D, thus

$$\sigma_{Nu} = \sigma_{Nu}(D) \tag{6.4.2}$$

At peak load we of course have the condition of equilibrium fracture propagation $\mathcal{G} = R$, which, with the aid of (6.4.1) and (6.4.2) can be written as

$$\mathcal{G}_u(\Delta a, D) = R(\Delta a) \quad \text{with} \quad \mathcal{G}_u(\Delta a, D) = \frac{D}{E'}\sigma_{Nu}^2(D)\, k^2\left(\alpha_0 + \frac{\Delta a}{D}\right) \tag{6.4.3}$$

Now, this equation holds for every D so that differentiting with respect to D we get

$$\frac{\partial \mathcal{G}_u(\Delta a, D)}{\partial D} = 0 \tag{6.4.4}$$

where the second member vanishes because, by hypothesis, the resistance curve depends only on Δa, not on D. Also, remark that α_0 must be taken as a constant upon differentiation because, by hypothesis, we are considering geometrically similar bodies.

Mathematically, the set of two equations (6.4.3) and (6.4.4) define the parametric equations of the envelope of the family of curves $\mathcal{G}_u(\Delta a, D)$. Elimination of D from the two sets of equations delivers $R(\Delta a)$.

Thus, it has been proven that the knowledge of the size effect law for a given geometry permits the determination of a unique *R*–curve (for that geometry). We now apply this property to Bažant's size effect law, first in an example, then in general form.

Example 6.4.1 Consider a double cantilever beam specimen as sketched in Fig. 6.4.1. Note that $a_0 = 10D$ so that $\alpha_0 = 10$ and all the specimens are geometrically similar. The expression for $\mathcal{G}$ found for this specimen in Chapter 2 —Eq. (2.1.28)— can be rewritten as

$$\mathcal{G} = 12\sigma_N^2 D(a/D)^2/E' \tag{6.4.5}$$

where D replaced h in the original equation and we defined the nominal stress as $\sigma_N = P/bD$. Comparing this to (6.4.1), we see that $k^2(\alpha) = 12\alpha^2$. If we further assume that Bažant's size effect law holds, so that $\sigma_{Nu} = Bf_t'(1 + D/D_0)^{-1/2}$, the energy release curve at peak load is given by:

$$\mathcal{G}_u(a) = \frac{(Bf_t')^2 D_0}{E'} \; \frac{D/D_0}{1 + D/D_0} 12 \left(\frac{a}{D}\right)^2 \tag{6.4.6}$$

We now substitute Bf_t' in terms of G_f using (6.2.3), and D_0 in terms of c_f using (6.2.2), for which we compute $2k_0'/k_0 = 2/\alpha_0 = 1/5$. The final expression for $\mathcal{G}_u(a)$ thus becomes

$$\mathcal{G}_u(a) = G_f \frac{5D/c_f}{1+5D/c_f}\left(\frac{a}{10D}\right)^2 = G_f \frac{5D/c_f}{1+5D/c_f}\left(1+\frac{\Delta a}{10D}\right)^2 \tag{6.4.7}$$

in which we set $a = a_0 + \Delta a$ and $a_0 = 10D$. Fig. 6.4.1 shows various $\mathcal{G}_u(a)$ curves for a number of sizes D plotted in a $\mathcal{G}/G_f$ vs $\Delta a/c_f$ plot. It is obvious that these curves define an envelope: the R–curve. To obtain the equation of the R–curve we set the partial derivative of (6.4.8) with respect to D equal to zero and solve for D. The result is

$$D = 2.5\frac{\Delta a}{c_f - \Delta a} \quad (0 \le \Delta a < c_f) \tag{6.4.8}$$

where the limitations in parenthesis simply state that neither Δa or D can be negative. Substitution of the foregoing equation into the expression (6.4.7) for $\mathcal{G}_u$ gives the equation for the R–curve:

$$R(\Delta a) = G_f \; 2\frac{\Delta a}{c_f}\left(1-\frac{\Delta a}{2c_f}\right) \quad (0 \le \Delta a < c_f) \tag{6.4.9}$$

Which is the arc of parabola OAM showing in Fig. 6.4.1. The R–curve is completed by a horizontal line $R(\Delta a) = G_f$ for $\Delta a \ge c_f$ a segment of which has been also drawn in the figure. □

6.4.2 R-Curve Determination Based on Bažant's Size Effect Law

The previous example deals with a very simple case in which the analytic determination of the R–curve is feasible. This is not generally the case, because of the complexity of the expressions for $k(\alpha)$ and its derivative. In the initial work of Bažant, Kim and Pfeiffer (1986), the R–curve was computed numerically. The numerical values of $\mathcal{R}$ so obtained were then fitted with an analytical expression. It was found that the expression $R(\Delta a) = G_f[1-(1-k\Delta a)^n]$ for $\Delta a < 1/k$ and $R(c) = G_f$ for $\Delta a \ge 1/k$, with optimized constants n and k, gave very good results. Subsequently, however, an analytical determination of the R–curve from the size effect law has been discovered (Bažant and Kazemi, 1990a). The method, which obtains the R–curve in explicit parametric form, is as follows.

According to Bažant's size effect law and the relation (6.2.3) between G_f and Bf_t', Eq. (6.4.2) can be explicitly written as

$$\sigma_{Nu}^2(D) = \frac{G_f E'}{k_0^2(D_0+D)} \tag{6.4.10}$$

Substitution in the second of (6.4.3) gives the expression for $\mathcal{G}_u(\Delta a, D)$

$$\mathcal{G}_u(\Delta a, D) = G_f \frac{D}{(D_0+D)k_0^2}\, k^2\left(\alpha_0 + \frac{\Delta a}{D}\right) \tag{6.4.11}$$

Before proceeding any further, it is convenient to define the parameter α' such that

$$\Delta a = (\alpha' - \alpha_0)D \tag{6.4.12}$$

The meaning of α' in this context is the value of $\alpha = a/D$ for which a specimen of size D reaches the peak load; thus, the straight solution of the problem would require solving for α' from the peak load condition to get the failure point for a given size. However, since we in general cannot solve for α', we circumvent the problem by writing every equation in terms of α' itself, i.e., using a parametric representation of all the equations in the problem.

The first equation to write is the tangency condition (6.4.4); thus, we differentiate (6.4.11) with respect to D, substitute Δa from (6.4.12) and solve for D; the result is

$$D = \frac{D_0 k(\alpha')}{(\alpha'-\alpha_0)2k'(\alpha')} - D_0 \tag{6.4.13}$$

which explicitly gives the size of the specimen that reaches the peak when $\alpha = \alpha'$. We substitute this value back into (6.4.12) and get Δa as a function of α'

$$\Delta a = \left[\frac{k(\alpha')}{2k'(\alpha')} - (\alpha' - \alpha_0)\right] D_0 \tag{6.4.14}$$

from which, inserting D_0 from expression (6.2.2), $D_0 = 2k_0' c_f / k_0$, we get the final expression for Δa

$$\frac{\Delta a}{c_f} = f_1(\alpha') = \left[\frac{k(\alpha')}{2k'(\alpha')} - (\alpha' - \alpha_0)\right] \frac{2k_0'}{k_0} \tag{6.4.15}$$

This equation gives the abscissa of the R–curve as a function of parameter α'. To get the ordinate, we solve for $\mathcal{R}$ by setting —in accordance with (6.4.3)— $\mathcal{R} = \mathcal{G}_u$, with $\mathcal{G}_u$ given by (6.4.11); after substituting D by its expression (6.4.13) and rearranging, the following expression for $\mathcal{R}$ is obtained:

$$\frac{\mathcal{R}}{G_f} = f_2(\alpha') = \frac{k(\alpha')k'(\alpha')}{k_0 k_0'} f_1(\alpha') \tag{6.4.16}$$

where $f_1(\alpha')$ is the function defined in (6.4.15). Eqs. (6.4.15) and (6.4.16) define the R–curve in explicit parametric form with parameter α' (Bažant and Kazemi, 1990a).

We note that the right hand sides of these equations depend only on geometrical properties ($k(\alpha')$ and its derivative); the only relevant material properties are G_f and c_f and they enter the equations by scaling, respectively, $\mathcal{R}$ and Δa. In fact, elimination of α' from the foregoing equations leads to an R–curve of the type

$$\frac{\mathcal{R}}{G_f} = f\left(\frac{\Delta a}{c_f}\right) \tag{6.4.17}$$

where function $f(\cdot)$ is completely defined by the shape of the specimen (including the initial relative notch depth).

In general, eliminating α' is not feasible analytically so that it is better to use the parametric form directly. To draw the R curve (scaled by G_f) we select a set of α' values. For each of them we evaluate $f_1(\alpha')$ from Eq. (6.4.15) and then calculate $f_2(\alpha')$ from Eq. (6.4.16). To obtain the R–curve for a particular material, the size effect method explained in the previous section is used to determine G_f and c_f and then the R–curve points $(\Delta a, \mathcal{R})$ for the various α' follow by setting $\Delta a = c_f f_1(\alpha')$ and $\mathcal{R} = G_f f_2(\alpha')$. Let us illustrate this by an example

Example 6.4.2 Consider the three-point bend specimens used by Bažant and Pfeiffer (1987) defined as series B1 and C1 in Table 1.1 and Fig. 1.5.1, and let us determine the R–curve. We use a graphics program to work out the curve. We first generate an array with various values of α', starting with $\alpha' = \alpha_0 = 1/6$; a selection of the evaluation points is shown in the fist row of the table below (in reality we use points spaced $\delta\alpha' = 0.005$, but there is no point in giving all the values here; the calculations for the 10 values shown can be obtained with a hand-held programmable calculator within reasonable time). The first step is to program function $k(\alpha')$ using the expressions (6.3.15) and (6.3.16). The function is run for the set of values α' and they are stored in a second array (the second row of the table). The third row contains the values of $k'(\alpha')$ which are obtained by calculating $k'(\alpha') \approx [k(\alpha' + 0.005) - k(\alpha' - 0.005)]/0.01$. Then, it is an easy matter to compute $\Delta a/c_f = f_1(\alpha')$ from (6.4.15) —fourth row of the table— and $\mathcal{R}/G_f = f_2(\alpha')$ from (6.4.16) —fifth row of the table.

α'	1/6	0.2	0.22	0.24	0.26	0.28	0.30	0.32	0.34	0.35
$k(\alpha')$	0.687	0.756	0.798	0.842	0.887	0.933	0.982	1.03	1.09	1.12
$k'(\alpha')$	2.10	2.10	2.14	2.20	2.29	2.39	2.52	2.67	2.85	2.95
$\Delta a/c_f$	1.00	0.897	0.815	0.720	0.614	0.498	0.375	0.244	0.109	0.039
$\mathcal{R}/G_f$	1.00	0.989	0.967	0.927	0.865	0.774	0.645	0.470	0.235	0.090

The dimensionless R–curve can be plotted by taking the fourth row as x-values and the fifth row as y-values. Such a plot is shown in Fig. 6.4.2 (the symbols indicate the points included in the table. The

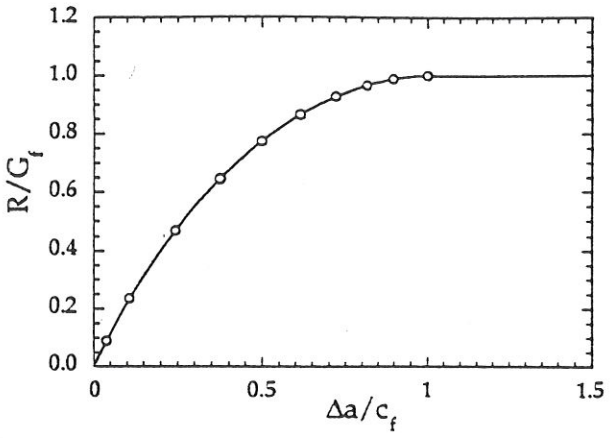

FIGURE 6.4.2
***R*–curve obtained from size effect for the three point bend notched beams tested by Bažant and Pfeiffer (1987). See Tables 1.1 and 1.2, and Fig. 1.5.2 for details.**

curve so obtained has parabolic form (as for the case in example 6.4.1) and is continued for $\Delta a/c_f > 1$ with a plateau $\mathcal{R} = G_f$. □

As is obvious from the foregoing examples, the R–curve obtained from the size effect law starts from zero, which means that the process zone forms right at the beginning of loading and that there is never any singularity at the mathematically sharp crack tip. (This type of R–curve is obtained by calculations from cohesive crack models with no nonlinearity in the surrounding material, or from crack bridging models that have no other toughening mechanism; Horii, Shi and Gong 1989; Elices and Planas 1992, 1993; Planas, Elices and Ruiz 1993). Some models for composite materials consider the R–curve to start from some initial non-zero value, interpreted as a certain small–scale value of the fracture energy. However, this kind of R–curve implies that the crack tip would be able to sustain, up to some value of the stress intensity factor, a singular stress field without showing any damage, which does not seem reasonable.

The R–curve obtained in this manner, as well as the load-deflection diagrams calculated from such R–curves, have been found to be in good agreement with numerous data on concrete and rocks, (Bažant and Kazemi, 1990a; Bažant, Gettu and Kazemi, 1991) as well as aluminum alloys (Bažant, Lee and Pfeiffer, 1987).

Determination of the R–curve from size effect data does not work in all circumstances. It obviously fails when $k'(\alpha_0) = 0$, and does not work when $k'(\alpha_0) \leq 0$, because $k'(\alpha_0) > 0$ ($D_0 > 0$) was implied in the derivation of Eq. (6.4.16). It also fails when $k'(\alpha_0)$ is too small, because of the scatter of test results. So this method must be limited to the positive specimen geometries, for which $k'(\alpha_0) > 0$. This nevertheless comprises most practical situations.

6.4.3 Determination of the Structural Response from the R–Curve

The determination of the load–displacement or load–CMOD curves for a particular specimen size once the R–curve has been determined as just explained is very easy. The first step is to determine the load corresponding to a point of the R–curve. Lets then assume that we have obtained a point $(\Delta a, \mathcal{R})$ as illustrated in the previous paragraph. The load corresponding to it for a static crack growth for a specimen of size D is obtained by setting $\mathcal{G} = \mathcal{R}$ or

$$\mathcal{R} = \frac{1}{E'}\sigma_N^2 D k^2(\alpha_0 + \Delta a/D) \tag{6.4.18}$$

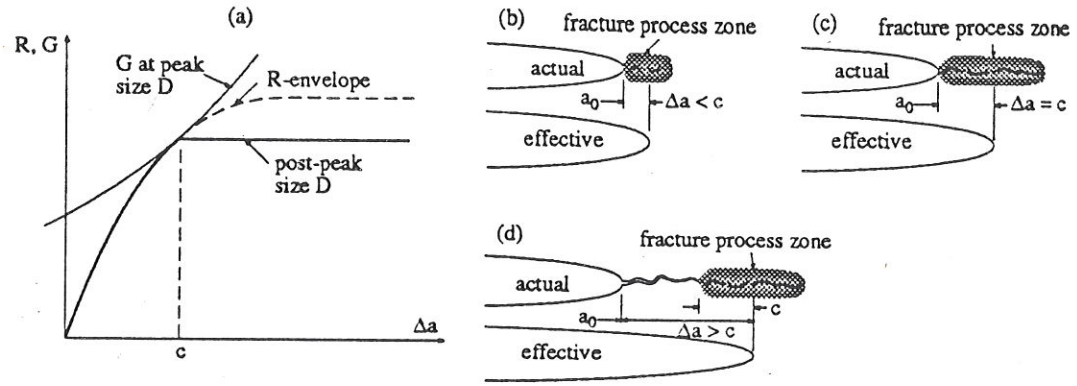

FIGURE 6.4.3
$\mathcal{R}$ is kept constant after peak load (a). Process zone at different stages: (b) before peak load; (c) at peak load; (d) after peak load. (Adapted from Bažant and Kazemi, 1990.)

which can be immediately solved for the load σ_N:

$$\sigma_N = \frac{\sqrt{E'\mathcal{R}}}{\sqrt{D}k(\alpha_0 + \Delta a/D)} \tag{6.4.19}$$

Now, the expression for the displacement u follows from (3.5.6) as

$$u = \frac{\sigma_N}{E'} Dv(\alpha_0 + \Delta a/D) \tag{6.4.20}$$

where $v(\alpha)$ can either be found in closed form in a handbook, or computed using (3.5.7), as derived in §3.5.1. Similar expressions can be used for the CMOD (see §3.5.3).

6.4.4 Bažant Modification of the Post-Peak Region of R–curves

When the R–curve given by Eqs. (6.4.14) and (6.4.16) is used in the calculation of the load–deflection curve, it must give, of course, maximum loads that exactly agree with the size effect law. This has been checked numerically. It has been also checked that such calculations give the correct shapes of the load–deflection diagrams up to the peak point (Bažant and Kazemi, 1990a,b). However, significant deviations from the observed load–deflection curves have been encountered in the post–peak regions for small specimens.

An explanation was sought and it was concluded that the foregoing calculation from the size effect law yields only a master R–curve whose entire length is followed only for a infinitely large specimen. In actual specimens, the master R–curve is followed only up to the maximum load point, after which one must assume, in order to get correct predictions of the post–peak deflection, that the value of R remains constant and equal to the value it reached at the peak load, i.e., the R–curve after the peak load is a horizontal line as depicted in Fig. 6.4.3a (Bažant, Gettu and Kazemi,1991; Bažant and Kazemi, 1990b). The reason for this behavior has not been firmly established, but apparently it consists in the fact that in the post–peak regime the fracture process zone, due to decreasing load, cannot keep growing; instead, it detaches itself from the tip of the notch or initial crack and travels forward without growing in size (see Fig. 6.4.3b–d).

6.4.5 Experimental Verification

According to the foregoing, the R–curve can be determined solely from the maximum load data on similar specimens of different sizes; for this curve to be useful, it has to be able to predict correctly the structural response, i.e., the load–deflection or load–CMOD curves. Whether this method gives realistic results has

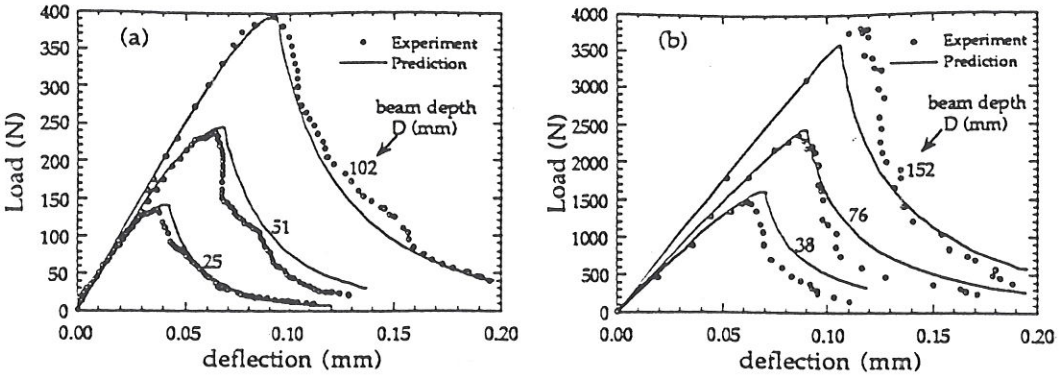

FIGURE 6.4.4
Size effect analysis of fracture tests on limestone: (a) Predicted and measured structural response for limestone specimens (After Bažant, Gettu and Kazemi 1991). (b) Predicted and measured structural response for high strength concrete specimens (After Gettu, Bažant and Karr 1990).

been investigated experimentally by Bažant, Gettu and Kazemi (1991) on limestone, and by Gettu, Bažant and Karr (1990) on high strength concrete. Three-point-bend specimens of different sizes were tested. The geometry of the specimens and the main properties of the materials are described in Tables 1.1 and 1.2 and in Fig 1.5.1 (series F1 and D1).

By regression of the maximum load data (Fig. 6.4.4a) the size effect law was calibrated, and then the R–curve was deduced according to method described. This R–curve was then used to calculate the diagram of the applied load vs. the load-line displacement. The predicted and measured load-deflection curves are shown in Fig. 6.4.4a for the limestone specimens and in Fig. 6.4.4b for the high strength concrete. Solid lines show the predicted curves, and the symbols represent the measured response.

In obtaining this deflection prediction, it was assumed that the master R–curve is followed only up to the peak load, and after that the R–value remains constant. Without this, the post peak deflection could not be predicted well. Moreover, the value of the elastic modulus used in the determination of the load deflection curve —Eqs. (6.4.19) and (6.4.20)— was not independently measured, but was adjusted to get a good fit of the initial slope. Thus, further analysis and tests are required for the model to be completely validated.

****

Exercises

6.7 Prove that for a double cantilever beam, the R–curve deduced from Bažant's size effect law is independent of the initial crack length.

6.8 Prove that for a crack of length $2a_0$ in an infinite panel subjected to uniform remote tensile stress, the envelope of the $\mathcal{G}_u(\Delta a)$ curves degenerates into a point of coordinates (c_f, G_f). Conclude that the R–curve can be considered to be defined by the segments of the limiting $\mathcal{G}_u(a)$ curves for $D = 0$ and $D = \infty$ which define the bilinear R–curve $R = G_f \Delta a / c_f$ for $0 \leq \Delta a \leq c_f$ and $R = G_f$ for $\Delta a \geq c_f$.

6.9 Find the R–curve based on Bažant's size effect (given G_f and c_f) for a double cantilever beam whose arms are subjected to a uniformly distributed load p per unit length. Take $\sigma_N = p/b$, $b =$ thickness, $D =$ arm depth, $a_0 = \alpha_0 D$.

6.10 Determine the load–displacement curve of the double cantilever beam analyzed in example 6.4.1 for the case $D = c_f/4$.

6.11 Determine the load–displacement curve of the double cantilever beam analyzed in example 6.4.1 for the case $D = c_f$.

6.12 Determine the load–displacement curve of the double cantilever beam analyzed in example 6.4.1 for the case $D = 4c_f$.

6.13 Show that the load–displacement curve expressed as a σ_N–u when the behavior is governed by an R–curve deduced from Bažant's size effect takes always the form

$$\sigma_N = \sigma_1 \phi\left(\frac{u}{u_1}, \frac{c_f}{D}\right), \quad \sigma_1 = \sqrt{\frac{E' G_f}{c_f}}, \quad u_1 = c_f \frac{\sigma_1}{E'} \tag{6.4.21}$$

where $\phi()$ is a non dimensional function, that depends implicitly on the shape only.

References

Bažant, Z. P. (6-1983) "Fracture in concrete and reinforced concrete," Preprints, IUTAM Prager Symposium on *Mechanics of Geomaterials: Rocks, Concretes, Soils*, ed. by Z. P. Bažant, Northwestern Univ., 281–316.

Bažant, Z. P. (6-1984) "Size effect in blunt fracture: Concrete, rock, metal." *J. of Engng. Mechanics*, ASCE, 110, 518–535.

Bažant, Z. P. (6-1986) "Fracture mechanics and strain-softening of concrete," in *Finite Element Analysis of Reinforced Concrete Structures*, C. Meyer and H. Okamura (Eds.), ASCE, New York, pp. 121–150.

Bažant, Z. P. (6-1987a) "Fracture energy of heterogeneous material and similitude" Preprints, *SEM-RILEM Int. Conf. on Fracture of Concrete and Rock* (held in Houston, Texas, June 1987), ed. by S. P. Shah and S. E. Swartz, publ. by SEM (Soc. for Exper. Mech.) pp. 390–402.??modernizar

Bažant, Z. P. (6-1987b). "Snapback instability at crack ligament tearing and its implication for fracture micromechanics." *Cement and Concrete Research* 17, 951–967.

Bažant, Z. P. (6-1989) "Identification of Strain-Softening Constitutive Equation from Specimens of Different Sizes," *Cement and Concrete Research*, Vol. 19 , pp. 973–977.

Bažant, Z. P. (6-199??) —discussion of Tang et al. (6-1992)

Bažant, Z. P. and Kazemi, M. T. (6-1990a). "Determination of fracture energy, process zone length and brittleness number from size effect, with application to rock and concrete," *Int. J. of Fracture*, 44, 111–131.

Bažant, Z. P. and Kazemi, M. T. (6-1990b). "Size effect in fracture of ceramics and its use to determine fracture energy and effective process zone length," *J. of American Ceramic Society* 73(7), 1841–1853.

Bažant, Z. P., and Kim, J-K. (6-1984). "Size effect in shear failure of longitudinally reinforced beams." *Am. Concrete Institute Journal*, 81, 456–468; Disc. & Closure 82 (6-1985), 579–583.

Bažant, Z. P. and Oh, B.-H. (6-1983). "Crack band theory for fracture of concrete," *Materials and Structures* (RILEM, Paris), 16, 155–177

Bažant, Z. P. and Pfeiffer, P. A. (6-1987). "Determination of fracture energy from size effect and brittleness number." *ACI Materials Jour.*, 84, 463–480.

Bažant, Z. P., Gettu, R., and Kazemi, M.T. (6-1991). "Identification of nonlinear fracture properties from size-effect tests and structural analysis based on geometry-dependent R-curves." *International Journal of Rock Mechanics and Mining Sciences*, 28(1), 43–51.

Bažant, Z. P., Kim, J-K. and Pfeiffer, P. A. (6-1986). "Nonlinear fracture properties from size effect tests." *J. of Structural Engng.*, ASCE, 112, pp. 289–307.

Bažant, Z. P., Lee, S-G, and Pfeiffer, P. A. (6-1987). "Size effect tests and fracture characteristics of aluminum." *Engng. Fracture Mechanics*, 26, (1), 45–57.

Brühwiller, E. (6-1988) "Fracture Mechanics of Dam Concrete Subjected to Quasi-Static and Seismic Loading Conditions," Laboratory of Building Materials (LMC), Swiss Federal Inst. of Tech., Lausanne, Thesis No. 739 (in German).

Chana, P. S., (6-1981) "Some Aspects of Modeling the Behavior of Reinforced Concrete Under Shear Loading," Technical Report No. 543, Cement and Concrete Association, Wexham Springs, pp. 22.

Cottrell, A. H. (6-1964) "The Mechanical Properties of Matter," John Wiley and Sons, New York.

Elices, M. and Planas, J. (6-1991) "Size effect and experimental validation of fracture models," in Analysis of Concrete Structures by Fracture Mechanics, L. Elfgren, Ed., Chapman and Hall, London, pp. 99–127.

Elices, M. and Planas, J. (6-1992) "Size Effect in Concrete Structures: an R-Curve Approach," in Applications of Fracture Mechanics to Reinforced Concrete, A. Carpinteri, Ed., Elsevier Applied Science, London, pp. 169–200.

Elices, M., and Planas, J. (6-1993) "The equivalent elastic crack: 1. Load-Y equivalences", *International Journal of Fracture*, **61**, pp. 159–172.

Gettu, R.,Bažant, and Karr, M. E. (6-1990). "Fracture properties and brittleness of high-strength concrete", *ACI Materials Journal*, 87 (Nov.-Dec.), pp. 608–618.

He, S., Plesha, M.E., Rowlands, R.E., and Bažant (6-1992) "Fracture energy tests of dam concrete with rate and size effects." *Dam Engineering* 3(2), 139–159.

Hillerborg, A. (6-1985) "The theoretical basis of method to determine the fracture energy G_F of concrete," *Materials and Structures*, Vol. 18, pp. 291–296.

Horii, H. (6-1989) "Models of Fracture Process Zone and a System of Fracture Mechanics for Concrete and Rock," Proc., Int. Workshop on Fracture Toughness and Fracture Energy, Sendai, Japan, pp. 325–337. ??modernizar

Horii, H., Hasegawa, A., and Nishino, F. (6-1989) "Fracture Process and Bridging Zone Model and Influencing Factors in Fracture of Concrete," in Fracture of Concrete and Rock, SEM/RILEM Int. Conf., Houston, eds. Shah, S. P., and Swartz, S. E., Springer-Verlag, New York, Berlin. pp. 205–214

Horii, H., Shi, Z., and Gong, S.-X. (6-1989) "Models of Fracture Process Zone in Concrete, Rock, and Ceramics,"in *Cracking and Damage, Strain Localization and Size Effect*, J. Mazars abd Z. P. Bažant (Eds.), Elsevier Applied Science, London, pp. 104–115.??ver pags

Iguro, M., Shioya, T., Nojiri, Y., and Akiyama, H. (6-1985) "Experimental Studies on Shear Strength of Large Reinforced Concrete Beams under Uniformly Distributed Load," Concrete Library Int., Japan Soc. of Civil Engrs., No. 5, pp. 137–154.

Karihaloo, B. L., and Nallathambi, P., 1991??, "Notched Beam Test: Mode I Fracture Toughness," in *??*, eds. ??, Chapman and Hall, London, pp. ??

Llorca, J., Planas, J. and Elices, M. (6-1989) "On the use of maximum load to validate or disprove models for concrete fracture behaviour," in Fracture of Concrete and Rock, Recent Developments, S. P. Shah et al. (Eds.), Elsevier, London, pp. 357–368.

Pastor, J. Y., Guinea, G., Planas, J. and Elices, M. (6-1995) "Nueva expresión del factor de intensidad de tensiones para la probeta de flexión en tres puntos," *Anales de Mecánica de la Fractura*, 12, in press. ("A new expression for the stress intensity factor of a three-point bend specimen." In Spanish.)

Planas, J., and Elices, M. (6-1989) "Size Effect in Concrete Structures: Mathematical Approximations and Experimental Validation," in *Cracking and Damage, Strain Localization and Size Effect*, J. Mazars abd Z. P. Bažant (Eds.), Elsevier Applied Science, London, pp. 462-476.

Planas, J. and Elices, M. (6-1990) "Anomalous structural size effect in cohesive materials like concrete", in Serviceability and Durability of Construction Materials, Vol. 2, B. A. Suprenant, Ed., American Society of Civil Engineers, ASCE, New York, pp. 1345–1356.

Planas, J. and Elices, M. (6-1991) "Nonlinear fracture of cohesive materials," International Journal of Fracture, 51, pp. 139–157.

Planas, J. and Elices, M. (6-1992) "A nonlinear analysis of a cohesive crack: 1. Theoretical background", International Journal of Fracture, 55, pp. 153-177.

Planas, J., Elices, M. and Ruiz, G. (6-1993) "The equivalent elastic crack: 2. X-Y equivalences and asymptotic analysis", *International Journal of Fracture*, **61**, pp. 231–246.

Press, W. H., Teukolsky, S. A., Vetterling, W. T. and Flannery, B. P. (6-1992) *Numerical Recipes in C*, Cambridge University Press, New York.

Pugh, E. M. and Winslow, G. H. (6-1966) *The Analysis of Phisical Measurements*, Addison-Wesley, Reading, Massachusetts.

RILEM (6-1985) "Determination of the fracture energy of mortar and concrete by means of three-point bend tests on notched beams," RILEM Draft Recommendation, TC 50-FMC Fracture Mechanics of Concrete. *Materials and Structures*, Vol. 18, pp. ??.

RILEM (6-1990) draft method based on size-effect.??

Saouma, V. E., Broz, J. J., Brühwiler, E., and Boggs, H. (6-1989) "Fracture Properties of Dam Concrete. Part I: Laboratory Experiments," submitted to J. of Mater. in Civil Engng., ASCE.??

Swartz, S. E., and Refai, T. M. E. (6-1989) "Influence of Size Effects on Opening Mode Fracture Parameters for Precracked Concrete Beams in Bending," in *Fracture of Concrete and Rock*, eds. Shah, S. P., and Swartz, S. E., SEM- RILEM Int. Conf., Houston, 1987, Springer-Verlag, pp. 242-254.

Tang, T., Shah, S.P., and Ouyang, C. (6-1992) "Fracture mechanics and size effect of concrete in tension", *J. of Structural Engineering*, ASCE , Vol. 118(11), Nov. 1992, 3169–3185.

Taylor, H. P. J. (6-1972) "The Shear Strength of Large Beams," J. of Struct. Engng., ASCE, pp. 2473–2490.

Tetelman, A. S. and McEvily, A. J. (6-1967) "Fracture of Structural Materials," John Wiley and Sons, New York, pp. 274–276.